

## ORIGINAL ARTICLE

# Electrical control of nanoscale functionalization in graphene by the scanning probe technique

Ik-Su Byun<sup>1,10</sup>, Wondong Kim<sup>2,10</sup>, Danil W Boukhvalov<sup>3,10</sup>, Inrok Hwang<sup>1,4</sup>, Jong Wan Son<sup>1</sup>, Gwangtaek Oh<sup>1</sup>, Jin Sik Choi<sup>1,5</sup>, Duhee Yoon<sup>6,7</sup>, Hyeonsik Cheong<sup>7</sup>, Jaeyoon Baik<sup>8</sup>, Hyun-Joon Shin<sup>8</sup>, Hung Wei Shiu<sup>9</sup>, Chia-Hao Chen<sup>9</sup>, Young-Woo Son<sup>3</sup> and Bae Ho Park<sup>1</sup>

Functionalized graphene is a versatile material that has well-known physical and chemical properties depending on functional groups and their coverage. However, selective control of functional groups on the nanoscale is hardly achievable by conventional methods utilizing chemical modifications. We demonstrate electrical control of nanoscale functionalization of graphene with the desired chemical coverage of a selective functional group by atomic force microscopy (AFM) lithography and their full recovery through moderate thermal treatments. Surprisingly, our controlled coverage of functional groups can reach 94.9% for oxygen and 49.0% for hydrogen, respectively, well beyond those achieved by conventional methods. This coverage is almost at the theoretical maximum, which is verified through scanning photoelectron microscope measurements as well as first-principles calculations. We believe that the present method is now ready to realize 'chemical pencil drawing' of atomically defined circuit devices on top of a monolayer of graphene.

*NPG Asia Materials* (2014) 6, e102; doi:10.1038/am.2014.24; published online 23 May 2014

**Keywords:** atomic force microscopy lithography; graphene; graphene functionalization; graphene hydrogenation; graphene oxidation; scanning photoelectron microscope; X-ray photoemission spectroscopy

## INTRODUCTION

Because functionalized graphene has distinguished physical<sup>1</sup> and chemical properties depending on functional groups<sup>2</sup> and their coverage,<sup>3</sup> it can be widely used for electronic,<sup>4</sup> chemical,<sup>5</sup> biological,<sup>6</sup> and optical<sup>7</sup> devices. Generally, chemical modifications are widely attempted in order to alter graphene's novel functionality.<sup>8–13</sup> However, conventional chemical modifications cannot selectively control functional groups on a well-defined target area. Moreover, it is important to fabricate freshly modified graphene with a low concentration of charge-scattering centers, which are usually induced by conventional fabrication or patterning methods.<sup>14</sup>

It has been reported that atomic force microscopy (AFM) lithography<sup>15</sup> can provide suitable methods of nanoscale chemical modification on a pristine graphene without any conventional source of surface contamination such as poly (methyl methacrylate). Because of its clean surface, the methods can be used for characterizing intrinsic chemical structures. If we verify the effect of voltage applied on derived functional groups during the modification, we can obtain an important tool to manipulate

the chemical structures of modified graphene on the nanoscale with a controllable parameter.

Among surface-sensitive techniques, X-ray photoemission spectroscopy (XPS) has been used for analyzing surface chemical composition and bonding. However, it is difficult to understand the local functional groups of modified graphene on the nanoscale<sup>16</sup> because the minimum analysis area ranges from 10 to 200  $\mu\text{m}^2$  (spot size).<sup>17</sup> A scanning photoelectron microscope (SPEM) equipped with scanning and focused X-ray of 200  $\text{nm}^2$  (spot size) is a powerful tool to investigate the local chemical structure. In this report, SPEM data for graphene oxidized by AFM lithography reveal a strong dependence of the ratio among functional groups (hydroxyl (C–OH), epoxy (C–O–C) and carbonyl (C=O)), and total oxygen coverage (up to 94.9%) on voltage applied during AFM lithography. Oxygen-containing functional groups on monolayer graphene can be almost removed by thermal annealing at 700 K in an ultra-high vacuum of  $10^{-9}$  Torr. The coverage of the hydrogen functional group can be raised up to 49.0% by AFM lithography and be fully removed by ultra-high vacuum annealing. Furthermore, first-principles

<sup>1</sup>Division of Quantum Phases and Devices, Department of Physics, Konkuk University, Seoul, Republic of Korea; <sup>2</sup>Division of Industrial Metrology, Korea Research Institute of Standards and Science, Daejeon, Republic of Korea; <sup>3</sup>School of Computational Sciences, Korea Institute for Advanced Study, Seoul, Republic of Korea; <sup>4</sup>Electronic Materials Research Center, Korea Institute of Science and Technology, Seoul, Republic of Korea; <sup>5</sup>Creative Research Center for Graphene Electronics, Electronics and Telecommunications Research Institute, Daejeon, Republic of Korea; <sup>6</sup>Department of Physics, Sogang University, Seoul, Republic of Korea; <sup>7</sup>Department of Electrical Engineering, University of Cambridge, Cambridge, UK; <sup>8</sup>Pohang Accelerator Laboratory, Pohang, Republic of Korea and <sup>9</sup>National Synchrotron Radiation Research Center, Hsinchu, Taiwan

<sup>10</sup>These authors contributed equally to this work.

Correspondence: Professor BH Park or Professor Y-W Son, Division of Quantum Phases and Devices, Department of Physics, Konkuk University, 1 Hwayang-dong, Kwangjin-gu, Seoul 143-701, Republic of Korea.

E-mail: baehpark@konkuk.ac.kr or hand@kias.re.kr

Received 6 November 2013; revised 3 February 2014; accepted 4 February 2014

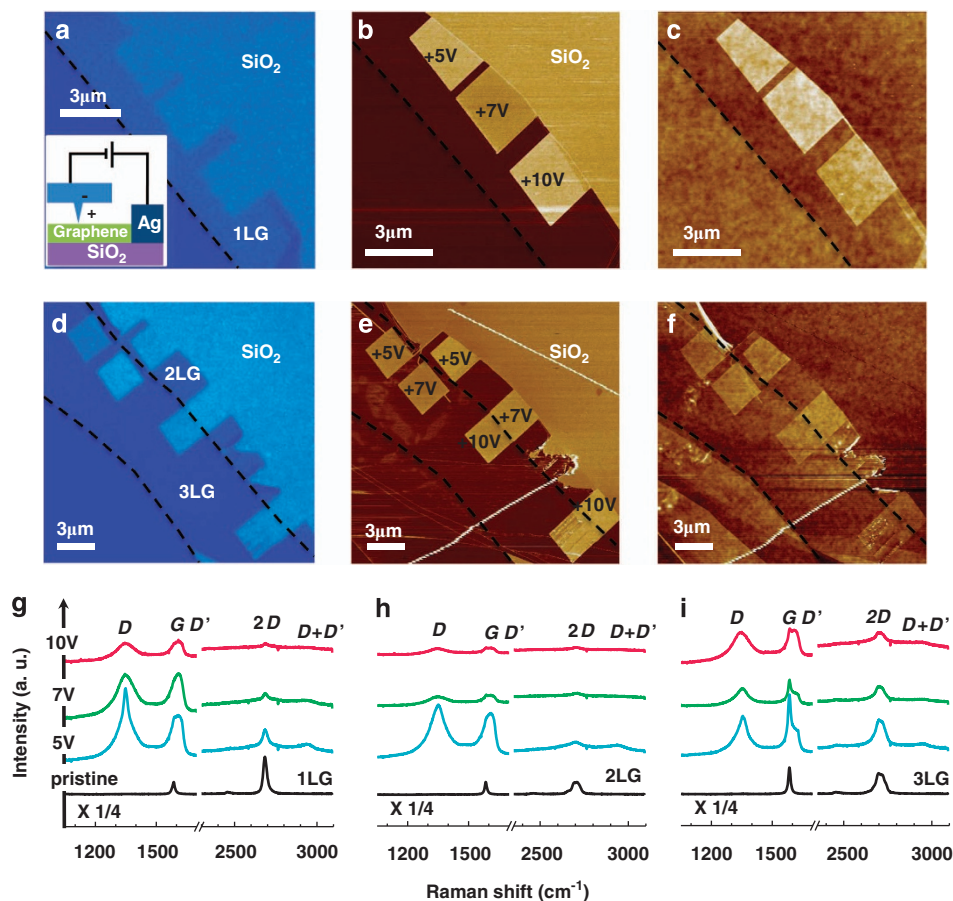


**Figure 1** Fabrication and characterization of the three oxidized areas on 1–3LG. (a–f) Optical microscope (a, d), friction force microscopy (FFM) (b, e) and topographic atomic force microscopy (AFM) (c, f) images of pristine and oxidized (using applied voltages of +5, +7 and +10V) 1–3LG. The inset in (a) shows the schematic setup of oxidation lithography using AFM. (g–i) Raman spectra of these pristine and oxidized 1LG (g), 2LG (h) and 3LG (i), respectively.

calculations support important experimental results, such as selective control of functional groups depending on the applied voltage or number of layers, irreversible oxidation of multilayer graphene and the maximum coverage of oxidation and hydrogenation. Our results reveal that AFM lithography is a simple method to design graphene nanodevices with controlled hydrogen- or oxygen-containing functional groups.

## MATERIALS AND METHODS

Graphene layers were prepared by the standard exfoliation method<sup>15</sup> as introduced in other papers, on thermally grown 300-nm-thick SiO<sub>2</sub> on a Si substrate. The graphene layers were identified by their color contrast under an optical microscope followed by thickness measurements using AFM and Raman spectroscopy.

The AFM lithography was performed at normal temperature and pressure by a contact-mode AFM (Nanofocus n-Tracer AFM system (Nanofocus, Seoul, Korea) and Parks System XE-100 (Park systems, Seoul, Korea)).<sup>15</sup> A Si cantilever with a Pt/Ir-coated conductive tip (Point Probe series, NANOSENSORS, Neuchatel, Switzerland) was used to apply a local dc bias voltage between a graphene sample and the conductive AFM tip. The spring constant and resonance frequency were set to 0.2 N m<sup>-1</sup> and 13 kHz, respectively. The relative humidity was maintained at around 30%, because it is very difficult to fabricate uniform and regular patterns on graphene under higher humidity condition where graphene is readily deformed. To avoid surface contamination from resist residues, electrode contact pads were formed using colloidal silver paste (TED PELLA, Redding, CA, USA), instead of the

conventional electron beam lithography technique.<sup>14</sup> To avoid the evaporation of silver paste, processing temperature of our sample was limited to 700 K.

The Raman spectra were obtained from locally modified squares ( $3 \times 3 \mu\text{m}^2$ ) with a micro-Raman system using the 514.5-nm line of an Ar ion laser as the excitation source. Other experimental details have been previously reported.<sup>18</sup>

SPEM measurements and micro-XPS were carried out at the U5 undulator beamline at the synchrotron radiation research center in Hsinchu, Taiwan, and 8A1 beamline of the Pohang Light Source, Pohang, South Korea. The detailed specifications of each beamline can be found in previous publications.<sup>19,20</sup> In both of the beamlines, a wide range of photon energy from 250 to 800 eV is available to collect photoelectrons from the sample using a hemispherical sector electron analyzer with multichannel detection (MCD) capability. The two-dimensional maps are obtained by scanning the sample with respect to the beam. The MCD scheme allows one to monitor different kinetic energies simultaneously. In the imaging mode, the sample is raster-scanned with respect to the photon beam, and the photoelectrons emitted from the beam spot on the sample are synchronously collected. Each pixel of the image corresponds to the intensity of the photoelectron signal at a particular place on the sample surface. The image represents the distribution of the photoelectron yield related to a specific chemical element, which is a measure for its local concentration. In addition, binding energy shifts can be used for mapping chemical states of each element on the sample surface. With the MCD capability, images of several different chemical states can be obtained in one scan, which can reduce the acquisition time drastically. The other mode of an SPEM system is photoemission spectroscopy from a small spot area, called micro-XPS. It is a detailed photoemission spectroscopic analysis of selected

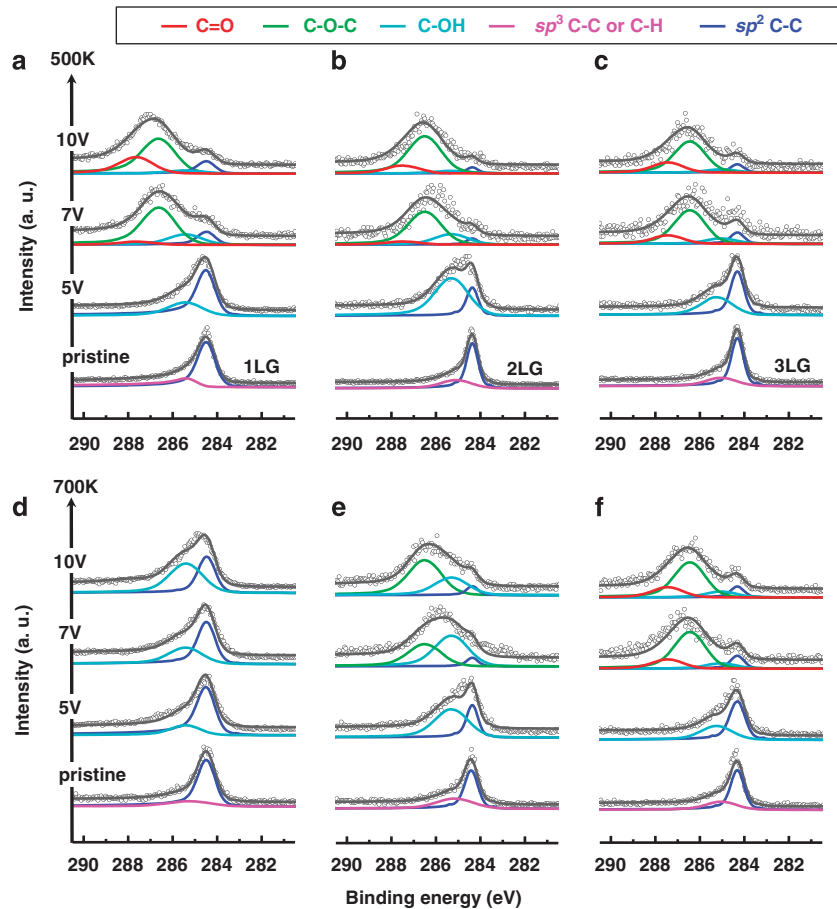


**Figure 2** Chemical states of pristine and oxidized 1–3LG. (a–c) X-ray photoemission spectroscopy (XPS) C 1s spectra of pristine and oxidized (using +5, +7 and +10V) 1LG (a), 2LG (b) and 3LG (c) after ultra-high vacuum (UHV) preannealing at 500K. (d–f) XPS spectra of 1LG (d), 2LG (e) and 3LG (f) after UHV annealing for 2 h at 700K. These were measured at the photon energy of 380 eV. The open circles and the gray line, respectively, reveal raw experimental data and the fitting result, which is the sum of the Shirley background (not shown).

areas, where the SPEM images show particularly interesting features. However, any unintentional charge accumulations on insulator can lead to an appreciable peak shift and misinterpretations. To avoid unintentional charge accumulation, which can be induced in the functionalized graphene area or the SiO<sub>2</sub> substrates by highly focused X-ray beam during SPEM measurement, we carefully prepared the ground electrode that is located outside the graphene. After cautious measurements with different incident beam intensities, we could confirm that the measured spectra were reproducible, and could exclude the possibility of peak shifts induced by the charging effect.

## RESULTS AND DISCUSSION

As shown in the inset of Figure 1, we have oxidized graphene on the nanoscale using AFM lithography with a positive-dc bias voltage<sup>15</sup> (positive AFM lithography) and scan speed of 0.1  $\mu\text{m s}^{-1}$ , which is chosen because non-uniform patterns are easily formed at higher scan speed. It is expected that oxides grow on graphene, which acts as an anode. In order to study the bias voltage effect, we oxidized areas ( $3 \times 3 \mu\text{m}^2$ ) with three bias voltages (+5 V, +7 V and +10 V) on monolayer (1LG), bilayer (2LG) and trilayer graphene (3LG), respectively, which were exfoliated mechanically on a SiO<sub>2</sub>/Si substrate. We can distinguish the nine oxidized areas from the pristine ones in the obtained optical microscope, friction force microscope and topographic AFM images (Figures 1a–f). The graphene oxidized with +5 V shows a height of 1.0 nm, whereas those oxidized with +7 V and +10 V reveal nearly saturated thickness

of 1.6 nm from the pristine one. We confirm the number of graphene layers by using Raman spectroscopy. In pristine 1–3LG, two prominent peaks (*G* and *2D*)<sup>21</sup> are clearly shown near 1580 and 2680  $\text{cm}^{-1}$  (Figures 1g–i), respectively. However, after oxidation, Raman *D*, *D'* and *D + D'* peaks appear near 1350, 1630 and 2940  $\text{cm}^{-1}$ , respectively, which are observed in *sp*<sup>3</sup> or disordered carbon networks<sup>22</sup> but not observed in pristine graphene. Oxidation of graphene is demonstrated by these defect-induced Raman peaks,<sup>15</sup> which are involved in symmetry broken *A*<sub>1</sub>' vibrational mode and cause the decreases of the *2D* band's intensity in oxidized graphene.<sup>15</sup> However, the Raman spectra do not provide information about the atomistic structures of the graphene oxidized by AFM lithography.

To investigate the functional groups induced by the positive AFM lithography, we have performed micro-XPS measurements using an SPEM system (Supplementary Figures S1 and S2). Figures 2a–c show the C 1s spectra obtained after preannealing treatment at 500 K and the fitting results of pristine and oxidized 1–3LG, respectively, formed by positive AFM lithography using +5 V, +7 V and +10 V (Supplementary Figure S3). For a quantitative approach, the area percentage, the normalized area ratio and the oxygen coverage are also calculated from the fitting results for the corresponding XPS spectra (Supplementary Figures S4 and S5). Energetics for such oxidation is obtained by first-principles calculations using the density functional theory, whose details are described in the Supplementary Information.

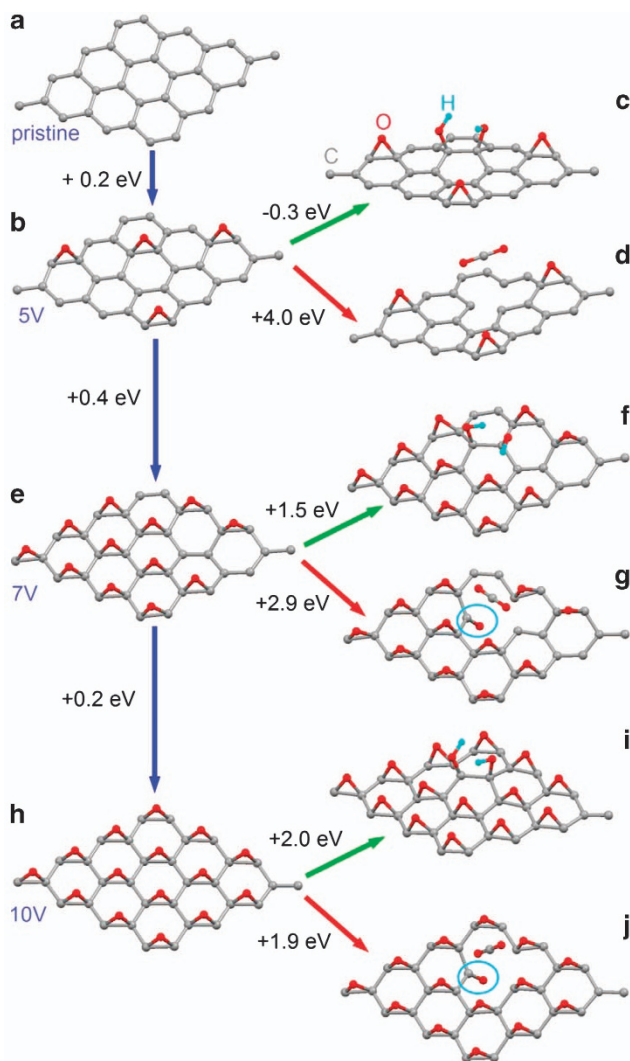


**Figure 3** Calculation results for oxidized 1LG. Atomic structures and formation energies of pristine graphene (a) and graphene supercells after first (b), second (e) and third (h) stage of chemisorption of oxygen corresponding with different applied voltages (see Supplementary Information), transformation of C–O–C group to C–OH (c, f and i), and activation of graphene vacancies with formation of CO<sub>2</sub> molecule (d, g and j) accompanied by further passivation of vacancies (g, j) using formation of C=O groups (blue circles).

For 1–3LG oxidized with +5 V, there are only two peaks (*sp*<sup>2</sup> C–C and C–OH): the area and intensity of *sp*<sup>2</sup> C–C are almost equal to those for pristine 1–3LG; considerable C–OH bonding is generated by the hydration of C–O–C groups (Figures 3b and c) in the presence of water similar to the reoxidation of reduced graphene oxide.<sup>23</sup> For 1LG, the energetic favorability of this process at a lower level of graphene oxidation corresponds with the transformation of all C–O–C groups to C–OH (Supplementary Figure S12). In particular, the formation energy of the C–OH groups for 2LG is higher than that for 1LG and 3LG.

For 1–3LG oxidized with +7 V, the areas of *sp*<sup>2</sup> C–C peaks are significantly reduced, C–OH peaks are slightly reduced and two additional oxygen-containing bonds (C–O–C and C=O) appear. We can argue that many *sp*<sup>2</sup> C–C bonds are broken by an external bias of +7 V and transformed into oxygen-containing bonds leading to a

high oxygen coverage. For 1LG, the appearance of C–O–C bonds implies that the energies required for the transformation of C–O–C to C–OH<sup>24</sup> are increasing with oxygen coverage (Figures 3e and f). Another effect of high oxygen coverage is the decreased energies required for the formation of vacancies on graphene, which are accompanied by the formation of carbon dioxide molecules (Figure 3d) and further passivation of dangling bonds with the formation of C=O groups (Figure 3g).

For 1–3LG oxidized with +10 V, the area of the oxygen-containing bonds generally increases, whereas that of *sp*<sup>2</sup> C–C is reduced. For 1LG, a significant increase in the C=O peak can be explained by the formation of more vacancies, which result from lower formation energies and are readily passivated by oxygen atoms (Figures 3h–j).

Remarkably, we observe high oxygen coverages of 2LG (94.9%) > 3LG (91.5%) > 1LG (88.1%) oxidized by positive AFM lithography using +10 V, which are significantly higher than that of graphene oxidized by the Hummers method<sup>8</sup> (79.0%). Because of the previously reported relation between oxygen coverage and the reduction of graphene oxide,<sup>25</sup> our highly oxidized graphene is expected to maintain a more regular carbon framework<sup>25</sup> after reduction than graphene oxidized by the Hummers method.<sup>8</sup>

The accessibility of oxygen ions to lower layers of graphene can be realized by perforation of the top layer, which was previously reported.<sup>26,27</sup> Our calculation (Supplementary Figure S12) demonstrates that for 1LG, the energy of oxidation is lower than that of vacancy formation for all levels of oxygen coverage. However, for 2LG and 3LG, the activation of vacancies on graphene can become energetically more favorable than further oxidation at a medium level of oxygen coverage. These results successfully elucidate a tendency to the formation of the perforations in the top layer, and oxidation of the second and further layers. Graphene samples with different numbers of layers show different amounts of the C–OH bond induced by +5 V: small, colossal and significant amounts on 1LG, 2LG and 3LG, respectively. These results can be explained by the different energetics of C–O–C and C–OH formation (Supplementary Figure S12). In the cases of multilayers, especially 2LG, formation of the C–OH bond on the oxidized top layer could also occur at a very high level of oxidation, whereas it is energetically unfavorable for significantly oxidized 1LG (Figures 3f and i). We should note that our first-principles calculations also reveal the possibility of totally oxidized graphene with the employment of C–O–C bonds caused by the low energy costs of this process independently from the number of layers (Figures 3b, e and h).

Figures 2d–f show the change in the C 1s spectra of pristine and oxidized 1–3LG after additional annealing at 700 K. The *sp*<sup>2</sup> C–C peak of all oxidized 1LG is significantly enhanced, and two peaks (C–O–C and C=O) almost disappear, which can be explained by the healing of graphene<sup>28</sup> through the decomposition of CO<sub>2</sub>, similar to its recently reported employment for graphene growth,<sup>27</sup> whereas the C–OH peak at +10 V still remains with significant intensity. We also confirmed AFM, friction force microscope and conductive AFM images on recovered 1LG (Supplementary Figure S6). Thus, we can argue that 1LG oxidized using low voltage returns nearly to the pristine 1LG through vacuum annealing at a temperature higher than 700 K. First-principles calculations also demonstrate the possibility of the removal of all oxygen atoms of one-sided graphene oxide because of the low binding energy between adatoms and the carbon substrate. Moreover, the combination method of vacuum annealing and photon-irradiation treatments seems to allow for further reduction and recovery of graphene oxidized by AFM lithography (Supplementary Figure S7).

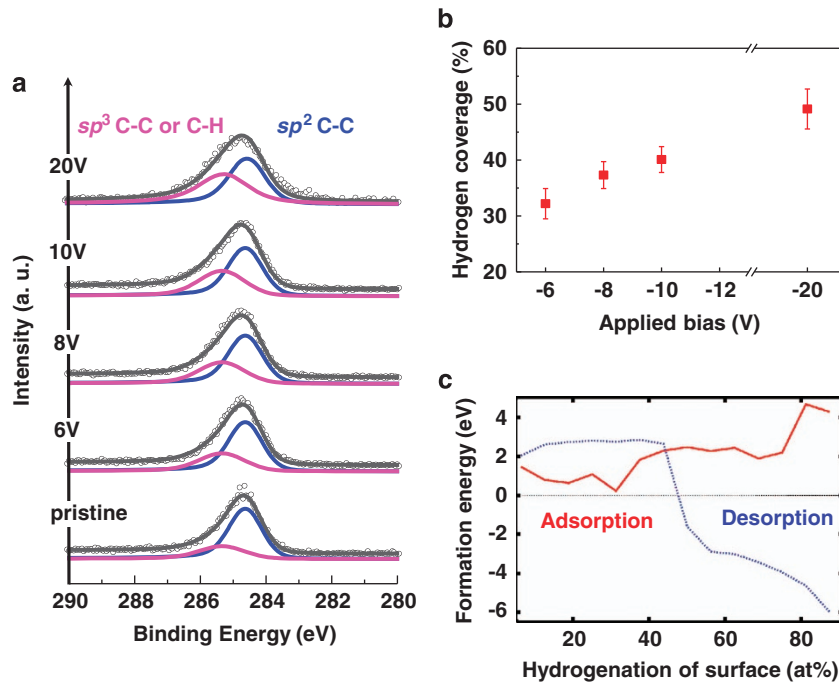


**Figure 4** Chemical states and calculation result of hydrogenated 1LG. (a) X-ray photoemission spectroscopy (XPS) C 1s spectra of pristine and hydrogenated (using  $-6$ ,  $-8$ ,  $-10$  and  $-20$  V) 1LG with calculated C 1s energies of  $sp^2$  C-C and  $sp^3$  (C-C or C-H) before ultra-high vacuum (UHV) annealing for 2 h at 500 K. The three hydrogenated 1LG samples reveal C 1s spectra fitted with two peaks: the main peak located at 284.5 eV with full width at half maximum (FWHM) of 1.05 eV is assigned to  $sp^2$  C-C peak in 1LG; the other peak at a higher binding energy (BE) with core-level shifts of 0.7 eV is assigned to that of  $sp^3$  (C-C or C-H,<sup>33</sup> or surface contamination on SiO<sub>2</sub><sup>34</sup>) peak. (b) Hydrogen coverage depending on electrical bias. (c) Energy of adsorption (solid red line) and desorption (dashed blue line) as a function of the hydrogenation of the graphene surface.

After annealing at 700 K, the C 1s spectra of 2LG do not show a large change, compared with that of 1LG. Furthermore, the spectra of 3LG exhibit little change. The irreversible oxidation of 2LG and 3LG can be explained by the protective coating of the top-most graphene.<sup>29</sup> The top-most layer of oxidized 2LG and 3LG can return partly to the pristine one by thermal effects and can be a protective film that hinders the penetration of gas molecules. If thermal reduction is induced at a lower layer of oxidized graphene, and oxygen gas is generated, then the local partial pressure of oxygen gas at the region between adjacent layers increases because of the protection of the top-most layer, and thus the following reduction is significantly suppressed. For oxidation, graphene oxidized using the conventional Hummers method<sup>8</sup> has contained various oxygen-containing functional groups, which have not been selectively controlled on the nanoscale yet.<sup>30</sup> By using positive AFM lithography, we can control the C-OH, C-O-C and C=O bonds at the surface of graphene. Because these oxygen-containing functional groups may affect the electrical (electrical properties of oxidized 1LG, Supplementary Figure S11a), chemical and optical properties<sup>1-8</sup> of oxidized graphene, positive AFM lithography can pave the way to designing graphene devices with controlled oxygen-functional groups.

Similar to the oxidized graphene, we have also hydrogenated 1LG on the nanoscale using negative AFM lithography, where a negative dc bias voltage is applied to the graphene<sup>15</sup> (Supplementary Figures S8 and S9). Because the hydrogen atom is prone to evaporate at 500 K, the hydrogenated 1LG was not preannealed at 500 K. Figure 4a shows the XPS C 1s spectra of pristine and the three hydrogenated 1LG, which are taken using SPEM. Figure 4b shows the hydrogen coverage (area of  $sp^3$  (C-C or C-H) divided by sum of areas for all the carbon bonds), which is estimated as 32.2%, 36.0% and 40.1% for 1LG hydrogenated with biases of  $-6$  V,  $-8$  V and  $-10$  V, respectively.

Furthermore, the hydrogen coverage can be increased to 49.0% on 1LG by using a higher bias of  $-20$  V. This implies that negative AFM lithography leads us to controlled hydrogen coverage on 1LG, which can reach a coverage higher (49.0%) than that induced by plasma treatment (16.6%).<sup>9</sup> After annealing at 500 K, hydrogenated graphene returns to a pristine one (Supplementary Figure S10), implying that hydrogen atoms can be completely dissociated by such thermal treatment.

For the hydrogenation process in modeling, we calculated the energies required for both adsorption of hydrogen atoms originating from decomposed molecular hydrogen<sup>31</sup> and desorption of hydrogen atoms from partially hydrogenated 1LG (Supplementary Figure S13). Our calculation demonstrates that one-sided hydrogenation should induce the formation of 'stripe-like' patterns (Supplementary Figure S13c) and will be stable for hydrogen concentrations below 44% (Figure 4c). Further hydrogenation requires significantly higher energies and induces unstable structures due to the desorption of hydrogen atoms. The obtained level of hydrogenation is in good agreement with experimental results and corresponds with the insulator structure (calculated band gap is 1.7 eV). Because the band gap of hydrogenated 1LG depends on hydrogen coverage,<sup>32</sup> we can engineer the electronic structure of hydrogenated 1LG in a wider range and enhance its applications in electronics (electrical properties of hydrogenated 1LG, Supplementary Figure S11b) and photonics by introducing negative AFM lithography.

In summary, we were able to manipulate the species and quantity of oxygen-containing and hydrogen-containing functional groups on the nanoscale by simply controlling the applied voltage during AFM lithography. Coverage of 94.9% for oxygen and 49.0% for hydrogen on graphene was achieved. 1LG modified by such AFM lithography can be almost completely recovered using ultra-high vacuum

annealing at 700 K. Furthermore, these experimental features were confirmed by first-principles calculations. Therefore, AFM lithography can provide a simple method to selectively control functional groups and thus the physical or chemical performance of graphene, leading to the development of graphene-based nanoscale devices.

## CONFLICT OF INTEREST

The authors declare no conflict of interest.

## ACKNOWLEDGEMENTS

This work was supported by the National Research Foundation of Korea (NRF) grants funded by the Korea government (MSIP) (No. 2013R1A3A2042120, 2011-0030228, 2008-0061893 (QMMRC) and 2011-0031640). Calculation is supported by the CAC of KIAS. The experiment at the NSRRC was supported by PAL through the abroad beam time program of the Synchrotron Radiation Facility Project under the MEST. I-SB was supported by a Hi Seoul Science/Humanities Fellowship from the Seoul Scholarship Foundation.

- Ramanathan, T., Abdala, A. A., Stankovich, S., Dikin, D. A., Herrera-Alonso, M., Piner, R. D., Adamson, D. H., Schniepp, H. C., Chen, X., Ruoff, R. S., Nguyen, S. T., Aksay, I. A., Prud'homme, R. K. & Brinson, L. C. Functionalized graphene sheets for polymer nanocomposites. *Nat. Nanotechnol.* **3**, 327–331 (2008).
- Englert, J. M., Dotzer, C., Yang, G. A., Schmid, M., Papp, C., Gottfried, J. M., Steinruck, H. P., Spiecker, E., Hauke, F. & Hirsch, A. Covalent bulk functionalization of graphene. *Nat. Chem.* **3**, 279–286 (2011).
- Hossain, M. Z., Johns, J. E., Bevan, K. H., Karmel, H. J., Liang, Y. T., Yoshimoto, S., Mukai, K., Koitaya, T., Yoshinobu, J., Kawai, M., Lear, A. M., Kesmodel, L. L., Tait, S. L. & Hersam, M. C. Chemically homogeneous and thermally reversible oxidation of epitaxial graphene. *Nat. Chem.* **19**, 305–309 (2012).
- Eda, G., Fanchini, G. & Chhowalla, M. Large-area ultrathin films of reduced graphene oxide as a transparent and flexible electronic material. *Nat. Nanotechnol.* **3**, 270–274 (2008).
- Elias, D. C., Nair, R. R., Mohiuddin, T. M. G., Morozov, S. V., Blake, P., Halsall, M. P., Ferrari, A. C., Boukhvalov, D. W., Katsnelson, M. I., Geim, A. K. & Novoselov, K. S. Control of graphene's properties by reversible hydrogenation. *Science* **323**, 610–613 (2009).
- Wang, Y., Li, Z. H., Wang, J., Li, J. H. & Lin, Y. H. Graphene and graphene oxide: biofunctionalization and applications in biotechnology. *Trends Biotechnol.* **29**, 205–212 (2011).
- Loh, K. P., Bao, Q., Eda, G. & Chhowalla, M. Graphene oxide as a chemically tunable platform for optical applications. *Nat. Chem.* **2**, 1015–1024 (2010).
- Stankovich, S., Piner, R. D., Chen, X. Q., Wu, N. Q., Nguyen, S. T. & Ruoff, R. S. Stable aqueous dispersions of graphitic nanoplatelets via the reduction of exfoliated graphite oxide in the presence of poly(sodium 4-styrenesulfonate). *J. Mater. Chem.* **16**, 155–158 (2006).
- Luo, Z., Yu, T., Kim, K.-j., Ni, Z., You, Y., Lim, S., Shen, Z., Wang, S. & Lin, J. Thickness-dependent reversible hydrogenation of graphene layers. *ACS Nano* **3**, 1781–1788 (2009).
- Yan, L., Zheng, Y. B., Zhao, F., Li, S., Gao, X., Xu, B., Weiss, P. S. & Zhao, Y. Chemistry and physics of a single atomic layer: strategies and challenges for functionalization of graphene and graphene-based materials. *Chem. Soc. Rev.* **41**, 97–114 (2012).
- Eigler, S., Hu, Y., Ishiibc, Y. & Hirscha, A. Controlled functionalization of graphene oxide with sodium azide. *Nanoscale* **5**, 12136–12139 (2013).
- Wu, C.-K., Wang, G.-J. & Dai, J.-F. Controlled functionalization of graphene oxide through surface modification with acetone. *J. Mater. Sci.* **48**, 3436–3442 (2013).
- Vasić, B., Kratzer, M., Matković, A., Nevesad, A., Ralević, U., Jovanović, D., Ganser, C., Teichert, C. & Gajić, R. Atomic force microscopy based manipulation of graphene using dynamic plowing lithography. *Nanotechnology* **24**, 015303–015312 (2013).
- Lin, Y.-C., Lu, C.-C., Yeh, C.-H., Jin, C., Suenaga, K. & Chiu, P.-W. Graphene annealing: how clean can it be? *Nano Lett.* **12**, 414–419 (2012).

- Byun, I. S., Yoon, D., Choi, J. S., Hwang, I., Lee, D. H., Lee, M. J., Kawai, T., Son, Y. W., Jia, Q., Cheong, H. & Park, B. H. Nanoscale lithography on monolayer graphene using hydrogenation and oxidation. *ACS Nano* **5**, 6417–6424 (2011).
- Li, Y. G., Zhou, W., Wang, H. L., Xie, L. M., Liang, Y. Y., Wei, F., Idrubo, J. C., Pennycook, S. J. & Dai, H. J. An oxygen reduction electrocatalyst based on carbon nanotube–graphene complexes. *Nat. Nanotechnol.* **7**, 394–400 (2012).
- Kim, S., Zhou, S., Hu, Y., Acik, M., Chabal, Y. J., Berger, C., De Heer, W., Bongiorno, A. & Riedo, E. Room-temperature metastability of multilayer graphene oxide films. *Nat. Mater.* **11**, 544–549 (2012).
- Yoon, D., Moon, H., Cheong, H., Choi, J. S., Choi, J. A. & Park, B. H. Variations in the raman spectrum as a function of the number of graphene layers. *J. Korean Phys. Soc.* **55**, 1299–1303 (2009).
- Klauser, R., Hong, I.-H., Lee, T.-H., Yin, G.-C., Wei, D.-H., Tsang, K.-L., Chuang, T. J., Wang, S.-C., Gwo, S., Zharnikov, M. & Liao, J.-D. Zone-plate-based scanning photoelectron microscopy at SRRC: performance and applications. *Surf. Rev. Lett.* **9**, 213 (2002).
- Lee, L. & Shin, H. J. Soft x-ray spectromicroscope at the pohang light source. *Rev. Sci. Instrum.* **72**, 2605–2609 (2001).
- Thomsen, C. & Reich, S. Double resonant Raman scattering in graphite. *Phys. Rev. Lett.* **85**, 5214 (2000).
- Saito, R., Jorio, A., Souza Filho, A. G., Dresselhaus, G., Dresselhaus, M. S. & Pimenta, M. A. Probing phonon dispersion relations of graphite by double resonance Raman scattering. *Phys. Rev. Lett.* **88**, 027401 (2002).
- Boukhvalov, D. W., Dreyer, D. R., Bielawski, C. W. & Son, Y.-W. A computational investigation of the catalytic properties of graphene oxide: exploring mechanisms by using DFT Methods. *ChemCatChem* **4**, 1844–1849 (2012).
- Boukhvalov, D. W. & Katsnelson, M. I. Modeling of graphite oxide. *J. Am. Chem. Soc.* **130**, 10697–10701 (2008).
- Marcano, D. C., Kosynkin, D. V., Berlin, J. M., Sinitskii, A., Sun, Z., Slesarev, A., Alemay, L. B., Lu, W. & Tour, J. M. Improved synthesis of graphene oxide. *ACS Nano* **4**, 4806–4814 (2010).
- Schniepp, H. C., Li, J.-L., McAllister, M. J., Sai, H., Herrera-Alonso, M., Adamson, D. H., Prud'homme, R. K., Car, R., Saville, D. A. & Aksay, I. A. Functionalized single graphene sheets derived from splitting graphite oxide. *J. Phys. Chem. B* **110**, 8535–8539 (2006).
- Zan, R., Ramasee, Q. M., Bangert, U. & Novoselov, K. S. Graphene reknits its holes. *Nano Lett.* **12**, 3936–3940 (2012).
- Luo, B., Liu, H., Jiang, L., Geng, D., Wu, B., Hu, W., Liu, Y. & Gui, Yu, G. Synthesis and morphology transformation of single-crystal graphene domain based on activated carbon dioxide by chemical vapor deposition. *J. Mater. Chem. C* **1**, 2990–2995 (2013).
- Prasai, D., Tuberquia, J. C., Harl, R. R., Jennings, G. K. & Bolotin, K. I. Graphene: corrosion-inhibiting coating. *ACS Nano* **6**, 1102–1108 (2012).
- Bagri, A., Mattevi, C., Acik, M., Chabal, Y. J., Chhowalla, M. & Shenoy, V. B. Structural evolution during the reduction of chemically derived graphene oxide. *Nat. Chem.* **2**, 581–587 (2010).
- Boukhvalov, D. W., Feng, X. & Müllen, K. First-principles modeling of the polycyclic aromatic hydrocarbons reduction. *J. Phys. Chem. C* **115**, 16001–16005 (2011).
- Gao, H., Wang, L., Zhao, J., Ding, F. & Lu, J. Band gap tuning of hydrogenated graphene: H coverage and configuration dependence. *J. Phys. Chem. C* **115**, 3236–3242 (2011).
- Nikitin, A., Li, X., Zhang, Z., Ogasawara, H., Dai, H. & Nilsson, A. Hydrogen storage in carbon nanotubes through the formation of stable C-H bonds. *Nano Lett.* **8**, 162–167 (2008).
- Kim, K. J., Lee, H., Choi, J. H., Yoon, Y. S., Choi, J., Kang, T. H., Jung, M. C., Shin, H. J., Lee, H. J., Kim, S. & Kim, B. Scanning photoemission microscopy of graphene sheets on SiO<sub>2</sub>. *Adv. Mater.* **20**, 3589–3591 (2008).



This work is licensed under a Creative Commons Attribution-NonCommercial-NoDerivs 3.0 Unported License. The images or other third party material in this article are included in the article's Creative Commons license, unless indicated otherwise in the credit line; if the material is not included under the Creative Commons license, users will need to obtain permission from the license holder to reproduce the material. To view a copy of this license, visit <http://creativecommons.org/licenses/by-nc-nd/3.0/>

Supplementary Information accompanies the paper on the NPG Asia Materials website (<http://www.nature.com/am>)